second-neighbor layers and between B and B' are included in the element P_{BB}. Also, the elements are normalized so that $\sum_{i,j} P_{ij} = 1$. One should notice that the asymmetry in P_{ij} does not violate microscopic reversibility; rather the inequality $P_{CB} > P_{BC}$ reflects the difference between "downhill" and "uphill" jumps between sites with different potential energies. It is also worthwhile to point out that although the relative magnitudes of the P_{ij} may be estimated approximately from static calculations of vacancy binding energies, molecular-dynamics simulation appears to be the only practical means of determining the absolute values of the P_{ij} and their temperature dependence for different sites.

In conclusion, we believe the present results provide the first detailed, microscopic evidence of the migration of vacancies in GB's. Some of the characteristics observed in our results are believed to be general features of the structure-dependent nature of grain-boundary diffusion. In Ref. 12 these molecular-dynamics data are combined with molecular-statics calculations to demonstrate further the vacancy-exchange mechanism for GB self-diffusion. Further simulations can be expected to yield additional information regarding the characteristics of different GB structures, and the dependence on interatomic potential functions of the diffusion dynamics and structural stability at various temperatures.

This work was supported in part by the Army Research Office, Contract No. DAAG-29-78-C-0006, by the U. S. Department of Energy, Contract No. DE-AS02-78-ER05002, and by the National Science Foundation, Grant No. DMR-78-12804.

[1]N. L. Peterson, in *Grain Boundary Structure and Kinetics* (American Society for Metals, Metals Park, Ohio, 1980), p. 209.

[2]R. W. Balluffi and J. W. Cahn, Acta Metall. 29, 493 (1981).

[3]C. H. Bennett, in *Diffusion in Solids*, edited by J. J. Burton and A. S. Nowick (Academic, New York, 1975), p. 73.

[4]A. DaFano and G. Jacucci, Phys. Rev. Lett. 39, 950 (1977).

[5]An attempt to calculate the vacancy migration energy in a 6° tilt boundary in α-iron with use of a quasidynamic method of simulation has been made by R. E. Dahl, J. R. Beeler, and R. D. Bourquin, in *Interatomic Potentials and Simulation of Lattice Defects*, edited by P. C. Gehlen, J. R. Beeler, and R. I. Jaffee (Plenum, New York, 1972), p. 673.

[6]A. Brokman, P. D. Bristowe, and R. W. Balluffi, to be published.

[7]R. A. Johnson, Phys. Rev. A 134, 1329 (1964).

[8]*Interatomic Potentials and Simulation of Lattice Defects*, edited by P. C. Gehlen, J. R. Beeler, and R. I. Jaffee (Plenum, New York, 1972).

[9]G. H. Bishop, R. J. Harrison, T. Kwok, and S. Yip, in *Progress in Materials Science*, Chalmers Anniversary Volume, edited by B. Chalmers, H. W. Christian, and T. B. Massalski (Pergamon, Oxford, 1981), p. 49.

[10]L. G. Harrison, Trans. Faraday Soc. 57, 1191 (1961).

[11]J. Bardeen and C. Herring, in *Imperfections in Nearly Perfect Crystals*, edited by W. Shockley *et al.* (Wiley, New York, 1952), p. 261; J. R. Manning, *Diffusion Kinetics for Atoms in Crystals* (Van Nostrand, Princeton, 1968).

[12]R. W. Balluffi, Thomas Kwok, P. D. Bristowe, A. Brokman, P. S. Ho, and Sidney Yip, to be published.

Laser-Induced Melt Dynamics of Si and Silica

M. A. Bösch and R. A. Lemons
Bell Laboratories, Holmdel, New Jersey 07733
(Received 21 April 1981)

Microscopic observations of blackbody emission from high-power cw-laser-irradiated silicon films on silica reveal: (I) Radiation of 1.06 μm produces a thermal runaway phenomenon in polycrystalline Si that terminates with the melt. (II) The laser-induced melt is inhomogeneous at the melting temperature. Lamellae of solid Si, which has a high emissivity, coexist with the low-emissivity melt. These lamellae transmit near-band-gap radiation, which is blocked by the molten phase, and they appear and disappear dynamically.

PACS numbers: 68.40.+e, 64.70.Dv, 81.40.-z

Laser crystallization of semiconductors on insulating substrates might emerge as an important technology in general and specifically for large-area Si electronics. It is important and interesting to understand the underlying mechanism for optically induced crystallization.

With pulsed laser irradiation both thermal melting and plasma annealing have been considered as mechanisms responsible for annealing of ion-implanted Si. How does a semiconductor react under extremely high optical excitation and consequently high electron-hole (e-h) generation rates? Is the energy rapidly transferred into the phonon system resulting in thermal melting,[1,2] or does an electronic process prevail where the high-density e-h plasma induces a second-order phase transition that allows the atoms to rearrange in a solid phase?[3-5] Recent experiments such as the transmission of near-band-gap radiation during the high-reflectivity period could be explained by plasma annealing only.[6] One might then ask whether an electronic process is partially involved in the cw-laser-induced melt dynamics.

In situ microscopic observations of the interaction region *directly* demonstrate the dynamics of thermal melting in Si films on silica substrates by cw-laser irradiation. (I) Blackbody emission (BBE) is observed as the Si heats and melts. The heating dynamics for irradiation just above the band-gap energy is manifest in a thermal runaway phenomenon which is terminated by the increase in reflectivity that occurs when the polycrystalline Si melts. (II) The laser-induced melt is inhomogeneous at the melting temperature. Solid Si lamellae that coexist with the melt appear and disappear *dynamically*. They transmit near-band-gap radiation which is blocked by the molten phase.

The laser pump sources used in this investigation were either an Ar^+-ion (0.5145 μm) or a Nd-yttrium aluminum garnet (Nd-YAlG) (1.064 μm) high-power cw laser. Polycrystalline and amorphous Si films with thickness between 0.4 and 1.0 μm were deposited on silica substrates by low-pressure chemical vapor deposition. Laser power in the range of 1–5 W will melt the silicon film on silica substrates when focused to a 50–300-μm-diam area. Microscopic observations were made with a research microscope equipped with visible or infrared sensitive television (TV) cameras and accompanying video recorder to allow analysis of the dynamic crystallization mechanism.[7]

The first observation is based on the dynamics of light absorption and heating of a polycrystalline Si film. Figure 1(a) shows the BBE intensity as a function of the laser intensity for photon energy twice the band-gap energy (Ar^+) and for photon energy slightly above the energy-gap (Nd-YAlG). In the former case increasing laser power heats the Si film and BBE is easily detected above 550°C. The enhanced absorptivity of the hot Si allows then more rapid heating towards the melting temperature (note arrow in curve). Raising the laser intensity slightly forces the film to melt. At that point the reflectivity of the melt is about 70% therefore lowering the heating rate considerably. Higher laser power will heat the melt only slightly and instead the higher energy flux forces the pool to enlarge. Eventually, the outward force due to the surface-tension gradient surpasses the capillary retention force leading to immediate hole formation in the Si film [$\approx$6 W in Fig. 1(a)]. The above description is slightly different for an amorphous film, since *a*-Si is transformed at 600°C into small-grain polycrystalline Si.

Heating with near-band-gap irradiation (Nd-YAlG) is strikingly different, and it is puzzling in the case of an *a*-Si film. Figure 1(a) shows the sharp threshold, above which melting of polycrystalline Si is exhibited. The hysteresis in the BBE as a function of laser intensity is indicative of a first-order phase transition since the BBE is a good temperature indicator. Although the absorption coefficient of *a*-Si is much higher than for polycrystalline Si, the maximum Nd-YAlG laser power available was insufficient to heat and melt an *a*-Si film. In the intermediate case of an electron-gun-evaporated film deposit-

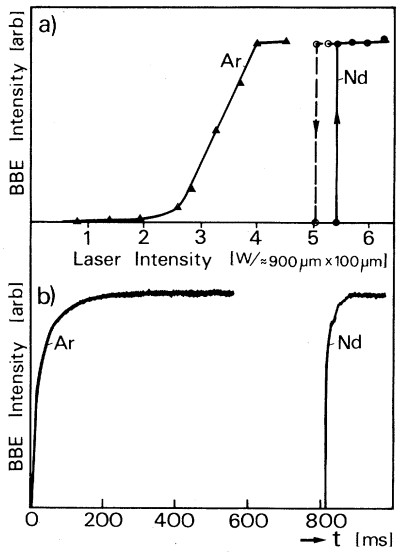

FIG. 1. Intensity of BBE from the laser heated area of a 1-μm polycrystalline Si film on silica (a) as a function of laser intensity in the steady state, (b) as a function of time starting with the onset of either Ar^+ or Nd-YAlG laser irradiation.

ed on a 550 °C substrate, periodic BBE was seen as the film was scanned relative to the laser beam.

In Fig. 1(b) we show the temporal behavior of the BBE for a 1.0-μm polycrystalline Si film after onset of laser power. The BBE increases rapidly with incident Ar^+ irradiation that will melt the film. However, for Nd-YAlG irradiation adjusted to the power threshold described above, there is a substantial delay before BBE is observed. Under very stable conditions, the delay was adjustable up to tens of seconds. This delayed onset of BBE is caused by a thermal runaway phenomenon that is terminated by the increase in reflectivity that occurs when the Si melts. This is the first direct observation of thermal runaway produced by near-band-gap radiation.

Thermal runaway effects have been suggested for both pulsed and cw CO_2-laser annealing.[8,9] For 10.6-μm radiation the mechanism is the thermal generation of free carriers (fc). This mechanism does not apply in our case since $\alpha_{fc} < 500$ cm^{-1} for 1.06-μm radiation even at the carrier concentration in Si at its melting point.[10] The only remaining absorption mechanism is by indirect transitions in the indirect-band-gap material. To substantiate our interpretation of the thermal runaway phenomenon, we calculate the temperature rise as a function of time. For this purpose we extend the laser-heating model of Ghez and Laff.[11] There the heat diffusion equation for a thin absorbing layer on a thick substrate is given for a temperature-independent laser flux F.

Solving the heat diffusion equation in one dimension simplifies the problem appreciably. Although this neglects the Gaussian laser beam profile and lateral diffusion, a useful approximation is achieved for short times. The major temperature dependence is supposed to be in the absorbed laser flux expressed as $F(T) = F_0(1-R)\{1 - \exp[-\alpha(T)d]\}$. R is the reflectivity of the film and $\alpha(T)$ is the temperature-dependent absorption coefficient. The absorption of a laser photon of $\hbar\omega = 1.17$ eV in an indirect-band-gap semiconductor such as Si requires absorption or emission of a phonon with energy $\hbar\Omega$ to provide the necessary momentum. We consider only the phonon absorption process, since it is dominant at room temperature and above. The indirect absorption is given by[12] $\alpha_a = A(\hbar\omega + \hbar\Omega - E_g)^2/p_\Omega$. The band-gap energy ($E_g$) is temperature dependent and we use the empirical expression[13]: $E_g(T) = E_g(0) - 7.02\times10^{-4}T^2/(T+1108)$. The temperature is given in degrees Kelvin and $E_g(0) = 1.16$ eV. The phonon population is described by $p_\Omega = \exp(\hbar\Omega/kT) - 1$. Over the temperature range of interest, the growing phonon population increases the absorption more than the narrowing of the band gap.

The constant A has been chosen to match the measured room temperature value $\alpha = 40$ cm^{-1}. From the phonon dispersion curves we select the highest energy transverse-optical phonon with $\hbar\Omega = 0.06$ eV, which contributes most to the absorption. With these values we generate the temperature-dependent absorption curve: For example, we find $\alpha_a = 10^4$ cm^{-1} at 1400 K. A solution of the heat diffusion equation with the temperature-dependent absorbed flux could be found numerically only.

The numerical solution for a uniform incident intensity of $F_0 = 5.1\times10^3$ W cm^{-2} can be approximated by two straight lines with slopes of 200 K/s and 8×10^4 K/s. They intersect at 0.9 s and 500 K. The initial gradual temperature rise of 340 K during 0.9 s is followed by a dramatic increase of 1000 K in only 30 ms. Since the BBE is very weak up to 800 K the initial gradual temperature increase is not observed. This delayed rapid heating describes the characteristic features of the observed thermal runaway in the Si film irradiated with the Nd-YAlG laser.

Numerical solutions for variable F_0 were also computed. Temperature values for an elapsed time of 1 s give then a numerical solution for the intensity threshold curve. This curve is also describable by two straight lines with slopes of 26 mK/W cm^{-2} and 12 K/W cm^{-2} and they intersect at 420 K and at an intensity of 4850 W cm^{-2}. The temperature stays remarkably low up to the crossing point but then the melting temperature is reached for an intensity increase of only 70 W/cm^2. This intensity fraction is of the same order as the stability of the laser. The numerical solutions show that our model successfully describes the observed features.

Further substantiation of a stable laser-induced melt is accomplished by microscopic observation of the BBE. With increasing laser power we gradually see the growing BBE intensity of the laser-heated area under the microscope. (In transmission microscopy the laser irradiated area darkens drastically due to the increased absorptivity before BBE sets in and dominates.) A sufficient increase of the laser intensity then induces a rapid appearance of a darker central area, the low emissivity melt, which is surrounded by a bright ring of hot solid Si of higher emissivity. A slight

increase of the laser intensity enlarges the central area which is interlaced with numerous bright lamellae as shown in Fig. 2(a). Observed in reflected light, as shown in Fig. 2(b), the melt is bright, manifesting its high reflectivity. At about 30% higher laser intensity the lamellae disappear and this state is necessary for the growth of crystallites a few hundred microns in size.

Figure 2(c) shows a high-resolution infrared TV micrograph of BBE filtered by a $\langle 100 \rangle$ c-Si wafer. The lamellae appear bright in the darker liquid. They change shape and position dynamically, and appear *identical* when viewed through the silica substrate at the silica-silicon interface. We believe that the high emissivity of the lamellae signifies their solid-state nature. These lamellae were seen in all types of available Si layers even when a *capping layer* of SiO_2 (0.5 μm) or Si_3N_4 was placed on top of the Si film. In the latter case the scanned trace is smooth and without ripples. Here it is appropriate to mention that lamellae were also observed in silicon on sapphire. For these samples, the lamellae grow predominantly along the crystal orientation of the substrate, therefore exhibiting epitaxial regrowth.

Transmission of near-band-gap radiation gives further evidence of solid lamellae formation. Figure 2(d) exhibits the same area of BBE as Fig. 2(c) but the middle portion shows the transmitted 1.15-μm radiation of a HeNe laser. Scanning the illuminated spot showed that no lag or blooming problems of the infrared sensitive vidicon were present. When the HeNe laser spot was scanned and centered at the boundary of the melt puddle no brightness difference between the lamellae and the adjoining solid Si was observable. Similar pictures were obtained if the visible part of the BBE was detected and 0.6328-μm laser light was transmitted through the lamellae.

As a result of the dynamical nature of the lamellae a final determination of their origin will have to await *in situ* microprobe analysis. We nevertheless speculate on the origin of an inhomogeneous melt and visualize two possible mechanisms to understand it: (i) Constitutional supercooling[14] can account for the growth of pure crystalline silicon lamellae coexisting with the melt. The melt has a lower temperature than Si since the impurities have segregated into it. (No material dependence was detectable though for the variety of Si films available.) Oxygen could be the predominant impurity, which would be acquired from either the ambient or the silica. According to the binary phase diagram of Si and O, pure Si is solidifying as the Si-O mixture is cooled along the liquidus curve. Solidification at the eutectic point produces eventually the two phases of solid Si and SiO_2. (ii) Phase separation in the pure Si melt might occur. A solid phase of fourfold coordinated Si clusters[15] could be surrounded by a metallic phase of liquid Si with no remaining covalent bonds.

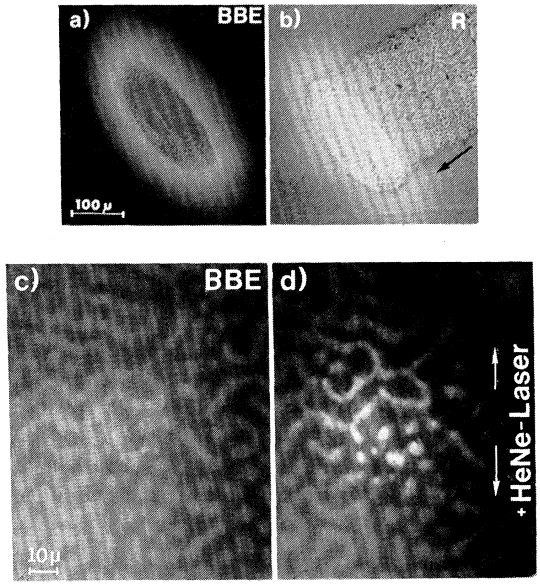

FIG. 2. (a) Visible-light micrograph of BBE from Ar^+-laser irradiated area. (b) Same as in (a) but viewed in reflected microscope light (R) showing high-reflectivity melt puddle and resolidified track; arrow indicates scan direction (wavelength range is 0.55 to 1.1 μm). (c) High-resolution infrared TV micrograph shows BBE from molten pool (wavelength range is 1.1 to 2 μm). (d) Same as in (c) but showing the transmission of a focused 1.15-μm HeNe laser beam.

In summary, we described observations that directly demonstrate heating and thermal melting of Si films on silica by cw-laser irradiation. *In situ* optical microscopy of the laser irradiated area showed an inhomogeneous melt occurring. Lamellae of solid Si coexist dynamically with the melt. This startling effect was neither predicted nor expected and its origin is not yet consistently understood. We suggest that pulsed-laser experiments similar to those we report for cw-laser irradiation would enhance the understanding of pulsed-laser annealing.

[1]P. Baeri, S. U. Campisano, G. Foti, and E. Rimini, Phys. Rev. Lett. 41, 1246 (1978).

[2]G. G. Bentini, C. Cohen, A. Desalvo, and A. V. Drigo, Phys. Rev. Lett. 46, 156 (1981).
[3]I. B. Khaibullin, E. I. Shtyrkov, M. M. Zaripov, R. M. Rayzitov, and M. F. Galayutdinov, Radiat. Eff. 36, 225 (1978).
[4]J. A. Van Vechten, Bull. Am. Phys. Soc. 26, 458 (1981); J. A. Van Vechten, R. Tsu, F. W. Saris, and D. Hoonhout, Phys. Lett. 74A, 417 (1979).
[5]H. W. Lo and A. Compaan, Phys. Rev. Lett. 44, 1604 (1980).
[6]M. C. Lee, H. W. Lo, A. Aydinli, and A. Compaan, Appl. Phys. Lett. 38, 499 (1981) and A. Aydinli, H. W. Lo, M. C. Lee, and A. Compaan, Phys. Rev. Lett. 46, 1640 (1981).
[7]M. A. Bösch and R. A. Lemons, Bull. Am. Phys. Soc. 26, 420 (1981).
[8]M. R. T. Siregar, W. Lüthy, and K. Affolter, Appl. Phys. Lett. 36, 787 (1980).
[9]G. K. Celler, R. Borutta, W. L. Brown, J. M. Poate, G. A. Rozgonyi, and T. T. Sheng, in *Laser-Solid Interactions and Laser Processing—1978*, edited by S. D. Ferris, H. J. Leamy, and J. M. Poate, AIP Conference Proceedings No. 50 (American Institute of Physics, New York, 1979), p. 381.
[10]A. Bhattacharyya and B. G. Streetman, Solid State Commun. 36, 671 (1980).
[11]R. A. Ghez and R. A. Laff, J. Appl. Phys. 46, 2103 (1975).
[12]J. I. Pankove, *Optical Processes in Semiconductors* (Prentice-Hall, Englewood Cliffs 1966).
[13]S. M. Sze, *Physics of Semiconductor Devices* (Interscience, New York, 1969).
[14]J. C. Phillips, private communication.
[15]V. M. Glazov, S. N. Chizhevskaya, and N. N. Glagoleva, *Liquid Semiconductors* (Plenum, New York, 1969).

Birefringence from Periodic Shear Flow near the Critical Point

Y. C. Chou and Walter I. Goldburg
Department of Physics and Astronomy, University of Pittsburgh, Pittsburgh, Pennsylvania 15260
(Received 7 August 1981)

The flow birefringence in the binary liquid mixture 2, 6-lutidine and water is measured near its critical point. The effect was produced by periodic variation of the shear, $S = \partial v_x/\partial y$, at an angular frequency, ω_0, of 7.5 $\sec^{-1}$, whereas typical average values of S were 10 $\sec^{-1}$. Measurements of the temperature dependence of the birefringence phase shift, δ, are in fair agreement with a steady-state theory of Onuki and Kawasaki.

PACS numbers: 64.60.Ht

It is well known that linearly polarized light becomes elliptically polarized on transmission through a sheared fluid containing nonspherical molecules.[1,2] According to a recent prediction, this effect, called flow birefringence, should also be observable in an isotropic fluid near its critical point.[3] Indeed there is one reported observation of this effect in a polystyrene-cyclohexane solution near its critical mixing temperature, though it was attributed to a pretransitional phenomenon in this complex polymer-solvent system.[4]

Here we report the first observation of critical flow birefringence in a fluid system whose critical parameters are known, so that the measurements can be compared with theory.[3] The central idea is that the shear flow in the fluid distorts the spontaneous critical fluctuations, whose average size ξ diverges at the critical point. These anisotropic fluctuations then play the role of nonspherical molecules in ordinary flow birefringence. From experimental[5] and theoretical investigations[6] over the last several years, we know that shear in critical systems also produces other dramatic effects, such as an azimuthal asymmetry in the light-scattering cross section, the replacement of Ising-model critical exponents by their mean-field values, and a shear-dependent shift in the critical temperature, T_c.[5,6]

In the present study, flow birefringence was measured under periodic shear at angular frequency ω_0. Two other frequencies which also appear are the local shear rate, $S = \partial v_x/\partial_y$, and the mean inverse lifetime, Γ_ξ, of the order parameter fluctuations. In our experiments, ω_0 was much smaller than Γ_ξ over most of the temperature range. Under this condition a steady-state analysis should approximate the experimental situation. Our results will be compared with the steady-state calculations of Onuki and Kawasaki in the weak shear regime ($S \ll \Gamma_\xi$).

The reader who is interested only in the results may glance ahead to Figs. 2(a) and 2(b), which are plots of the peak birefringence angle δ_m vs $\Delta T \equiv T_c - T$ in a critical mixture of 2, 6-lutidine and water; the data refer to two values of S. The

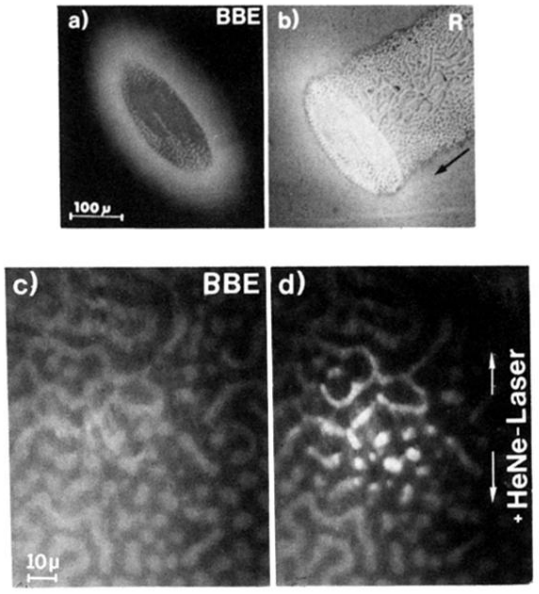

FIG. 2. (a) Visible-light micrograph of BBE from Ar^+-laser irradiated area. (b) Same as in (a) but viewed in reflected microscope light (R) showing high-reflectivity melt puddle and resolidified track; arrow indicates scan direction (wavelength range is 0.55 to 1.1 μm). (c) High-resolution infrared TV micrograph shows BBE from molten pool (wavelength range is 1.1 to 2 μm). (d) Same as in (c) but showing the transmission of a focused 1.15-μm HeNe laser beam.